

DINO-Mix: Distilling Foundational Knowledge with Cross-Domain CutMix for Semi-supervised Class-imbalanced Medical Image Segmentation

Xinyu Liu¹, Guolei Sun²

¹The Chinese University of Hong Kong

²College of Computer Science, Nankai University

xinyuliu@link.cuhk.edu.hk, guolei.sun@nankai.edu.cn

Abstract

Semi-supervised learning (SSL) has emerged as a critical paradigm for medical image segmentation, mitigating the immense cost of dense annotations. However, prevailing SSL frameworks are fundamentally “inward-looking”, recycling information and biases solely from within the target dataset. This design triggers a vicious cycle of confirmation bias under class imbalance, leading to the catastrophic failure to recognize minority classes. To dismantle this systemic issue, we propose a paradigm shift to a multi-level “outward-looking” framework. Our primary innovation is Foundational Knowledge Distillation (FKD), which looks outward beyond the confines of medical imaging by introducing a pre-trained visual foundation model, DINOv3, as an unbiased external semantic teacher. Instead of trusting the student’s biased high confidence, our method distills knowledge from DINOv3’s robust understanding of high semantic uniqueness, providing a stable, cross-domain supervisory signal that anchors the learning of minority classes. To complement this core strategy, we further look outward within the data by proposing Progressive Imbalance-aware CutMix (PIC), which creates a dynamic curriculum that adaptively forces the model to focus on minority classes in both labeled and unlabeled subsets. This layered strategy forms our framework, DINO-Mix, which breaks the vicious cycle of bias and achieves remarkable performance on challenging semi-supervised class-imbalanced medical image segmentation benchmarks Synapse and AMOS.

Introduction

The accurate delineation of anatomical structures and pathologies in medical imaging is a cornerstone of modern diagnostics, treatment planning, and clinical research. While deep learning models have demonstrated remarkable capabilities for this task (Li et al. 2025), their performance is heavily contingent on vast amounts of meticulously annotated data. The creation of such datasets is a notorious bottleneck, requiring expert knowledge and significant time. This reality has propelled semi-supervised learning (SSL) to the forefront of medical imaging research (Han et al. 2024), offering a promising path to leverage large, readily available cohorts of unlabeled data alongside small, annotated sets.

Copyright © 2026, Association for the Advancement of Artificial Intelligence (www.aaai.org). All rights reserved.

Despite its promise, the dominant paradigm in semi-supervised learning is architecturally “inward-looking.” Methodologies ranging from classic consistency-based approaches (Yu et al. 2019; Wu et al. 2022; Luo et al. 2021b; Liu, Chen, and Yuan 2024) to more recent, sophisticated frameworks all manage to refine information generated entirely from the target dataset’s statistics. This design exposes a fatal vulnerability in the face of class imbalance, which is a condition endemic to medical imaging, where small lesions or organs are vastly outnumbered by background tissues or organs with large size. Although some recent works have been proposed to address the class-imbalance issue with selective self-training (Wei et al. 2021) or co-training (Wang and Li 2023a; Zhang et al. 2025), they remain operating within the inward-looking paradigm, and would suffer from the vicious cycle of confirmation bias (Arazo et al. 2020). This process begins with an initial model preference for the over-represented majority class. The model then generates pseudo-labels predicated on its own biased confidence, which are overwhelmingly skewed. Eventually, the model trained on its own prejudiced predictions will further cement its initial bias and progressively starve minority classes of supervisory signals until they are completely ignored.

We posit that any attempt to mitigate this cycle from within is fundamentally limited. The solution requires a paradigm shift: from an “inward-looking” to an “outward-looking” philosophy that introduces objective, external knowledge immune to the dataset’s skewed statistics. Our primary contribution, Foundational Knowledge Distillation (FKD), which actualizes this philosophy by looking outward beyond the entire domain of medical imaging. We introduce a pre-trained visual foundation model DINOv3 (Siméoni et al. 2025) as a frozen unbiased external semantic teacher. Having learned from millions of diverse, natural images via self-supervision, DINO’s representations are not tied to any specific downstream task or class distribution. Its understanding is based on universal principles of visual distinctiveness—texture, shape, and structure. By distilling its robust feature representations into our segmentation student, we provide a stable, objective supervisory signal. This external anchor, grounded in visual salience rather than class frequency, directly counteracts the vicious cycle. When the student model is uncertain about a rare but visually distinct lesion, our foundational model provides guid-

ance with a strong, persistent gradient, ensuring the student learns its features.

To complement the powerful cross-domain guidance from the DINO teacher, we introduce a second, input-level “outward-looking” mechanism designed to build a more receptive student model named Progressive Imbalance-aware CutMix (PIC), which institutes a dynamic learning curriculum that evolves over the course of training. In the initial stages, when the model is most susceptible to the dataset’s inherent bias, PIC operates in a heavily class-aware mode. It aggressively samples and pastes regions from minority classes, forcing the student to immediately confront and prioritize learning from the most challenging and underrepresented examples. As training matures and the model develops a more balanced understanding, PIC progressively relaxes this constraint, transitioning its sampling strategy towards a uniform distribution. This strategic shift prevents overfitting on minority classes and ensures the student builds robust features for the entire dataset. By first tackling the core data imbalance and then generalizing, PIC cultivates a more competent student, ideally prepared to absorb and leverage the profound knowledge distilled from its foundational teacher.

The synergy between these two components forms a cohesive and powerful framework named *DINO-Mix*. The external teacher provides the unbiased *what* to learn, breaking the semantic bias loop, while the adaptive intra-domain regularizer creates a more robust student that is better at *how* to learn, especially for rare classes. This two-pronged “outward-looking” attack dismantles the vicious cycle of confirmation bias at its root. Through extensive experiments on the highly imbalanced Synapse and AMOS datasets, we demonstrate that our approach not only resolves a critical failure mode of existing SSL methods but also sets a new state-of-the-art in semi-supervised medical image segmentation. The main contributions of our work include:

- We propose a novel “outward-looking” paradigm Foundational Knowledge Distillation (FKD) for semi-supervised medical segmentation by leveraging a pre-trained foundation model DINOv3 as an external, unbiased semantic teacher, which provides a stable supervisory signal for minority classes.
- We introduce Progressive Imbalance-aware CutMix (PIC), a dynamic intra-domain regularization strategy that constructs a learning curriculum, beginning with a class-aware focus and progressively shifting to uniform sampling to build a robust and generalized student model.
- We combine these components into a cohesive framework, DINO-Mix, which achieves new state-of-the-art results on challenging and highly imbalanced semi-supervised segmentation benchmarks.

Related Work

Semi-supervised Medical Image Segmentation

Semi-supervised medical image segmentation (SSMIS) addresses the scarcity of labeled medical data, especially in 3D imaging like ultrasound and MRI, by leveraging large

pools of unlabeled scans (Yu et al. 2019; Luo et al. 2021a,b; Liu, Chen, and Yuan 2024; Liu, Li, and Yuan 2024; Chen et al. 2021). The field has evolved along two main, often intertwined, approaches: consistency regularization and pseudo-labeling. In consistency regularization, models are trained to produce invariant predictions on perturbed inputs of the same unlabeled data, often within a teacher-student framework. Methods like Mean Teacher (Tarvainen and Valpola 2017) and its medical adaptation UA-MT (Yu et al. 2019) employ EMA and uncertainty weighting, while URPC (Luo et al. 2021b) and DTC (Luo et al. 2021a) introduce multi-level feature and dual-task constraints to improve boundary quality. The pseudo-labeling branch generates targets from the model’s own confident predictions, as seen in FixMatch (Sohn et al. 2020). To mitigate error accumulation, co-training architectures like Cross Pseudo Supervision (CPS) (Chen et al. 2021) were proposed, where two networks provide mutual supervision to correct each other’s mistakes. Some recent approaches have been exploring more diverse data transformations including copy-paste augmentation (Bai et al. 2023) and frequency domain interpolation (Hu et al. 2025). However, these methods are fundamentally “inward-looking”, as they rely entirely on supervisory signals generated from within the training process itself. This could create a vulnerability to confirmation bias when extended to multi-organ segmentation tasks, where an initial preference for majority classes is rapidly amplified, leading to the neglect of minority structures.

Semi-supervised Class-imbalanced Learning

A fundamental challenge in real-world medical imaging is class imbalance, which impairs model generalization, especially for rare classes (Wang and Li 2023a; Li, Liu, and Chen 2024; Zhang et al. 2025; Sohn et al. 2020; Yang et al. 2022). This issue is magnified in semi-supervised learning, which is due to the scarcity of labeled examples for minority classes. Recent research has developed specialized SSL methods to tackle this challenge. Some focus on creating a balanced training set using pseudo-labels, such as CReST (Wei et al. 2021), which explicitly selects pseudo-labeled data to favor minority classes. Others adjust the learning dynamics directly: CLD (Lin et al. 2022) re-weights the loss based on class instance counts, while DHC (Wang and Li 2023a) advances this by considering both class distribution and learning difficulty. GenericSSL (Wang and Li 2023b) extracts distribution-invariant features from aggregated information from multiple distributions/domains. SKCDF (Zhang et al. 2025) adopts labeled data to guide the generation of pseudo labels in feature level via a cross-attention mechanism. However, these approaches are confined to the data distributions within the dataset itself, which may be still restricted by the limited semantics and representations.

Leveraging Foundational Models for Semi-supervised Learning

The advent of foundational models, pre-trained on vast labeled or unlabeled datasets, has revolutionized the field of computer vision by learning robust and highly generalizable representations (Radford et al. 2021; Oquab et al. 2023;

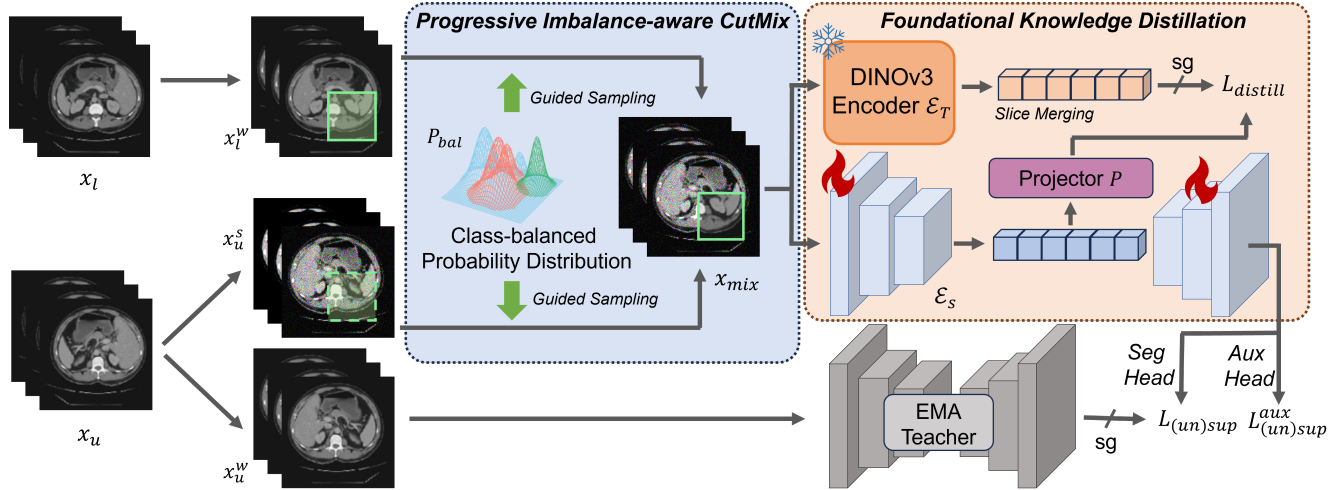


Figure 1: The overview of our proposed DINO-Mix framework for semi-supervised class-imbalanced medical image segmentation during training, which includes two main components Progressive Imbalance-aware CutMix (PIC) and Foundational Knowledge Distillation (FKD).

Siméoni et al. 2025). Their profound ability to understand semantic content from unlabeled data makes them exceptionally well-suited for SSL, where the scarcity of labeled data is a primary challenge (Li et al. 2024; Huang et al. 2025; Pham et al. 2025; Hoyer et al. 2024; Li, Huang, and Guan 2025). This methodology has been validated across diverse and complex domains. For instance, Hoyer et al. (Hoyer et al. 2024) proposed SemiVL, a method that integrates rich semantic priors from a CLIP model to resolve ambiguities between visually similar classes, a common failure point for traditional SSL that rely solely on visual consistency. The application of this principle extends even to more nuanced scenarios, such as fine-grained open-set SSL, where Li et al. (Li, Huang, and Guan 2025) employ a CLIP-driven, coarse-to-fine framework to progressively focus on distinctive visual details. In the task of 3D semantic scene completion, Pham et al. (Pham et al. 2025) introduce a framework that utilizes depth and segmentation foundation models to extract geometric and semantic 3D clues from unlabeled images. However, a common thread in these pioneering efforts is their significant reliance on vision-language models (e.g., CLIP) or task-specific foundation models. While highly effective, this focus has left the potential of purely vision-based self-supervised foundational models, which learn powerful semantic representations through self-supervised objectives without any textual data or task-specific labels. They are relatively underexplored in the context of SSL guidance. Models like DINO family, for instance, have shown an exceptional ability to learn object-level features and semantic segmentation maps directly from images. Yet, their direct integration as semantic teachers within semi-supervised frameworks remains a nascent area.

Methodology

Our DINO-Mix framework is built upon a consistency regularization paradigm (Sohn et al. 2020; Liu, Chen, and Yuan 2024) with an Exponential Moving Average (EMA) teacher model to generate stable pseudo-labels, as illustrated in Fig. 1. For unlabeled data, we generate a weakly-augmented view and a strongly-augmented view. The EMA teacher model produces a high-confidence pseudo-label from the weakly-augmented view, which then serves as a supervision target for the prediction from the strongly-augmented view, enforcing model consistency. Moreover, an auxiliary balancing classifier (Lee, Shin, and Kim 2021; Zhang et al. 2025) is applied to disentangle the learning of general representations from the specific task of handling class imbalance. Into this baseline, we integrate a two-pronged “outward-looking” strategy. First, we introduce an external, pre-trained foundation model as a source of unbiased semantic knowledge to break the cycle of confirmation bias. Second, we employ a novel intra-domain data mixing strategy to regularize the student model and enhance its generalizability.

Foundation Knowledge Distillation (FKD)

The fundamental flaw of conventional semi-supervised learning is its susceptibility to a vicious cycle of confirmation bias. When faced with class imbalance, a student model’s initial preference for the majority class leads it to generate biased pseudo-labels. Training on these self-generated flawed targets causes the model to become increasingly confident in its own errors, progressively starving minority classes of a supervisory signal until they are ignored entirely. To break this destructive feedback loop, an “outward-looking” approach that introduces a source of supervision completely external to the student model and immune to the dataset’s skewed statistics. To realize this external semantic anchor, we employ a pre-trained DINOv3 Vision Transformer, with its encoder denoted as \mathcal{E}_T ,

which remains frozen throughout training. Having learned from millions of diverse, non-medical images, the pre-trained DINOv3 encoder \mathcal{E}_T possesses a rich, task-agnostic understanding of fundamental visual concepts, making it an ideal objective teacher. We transfer this knowledge to our 3D segmentation student, whose encoder is denoted as \mathcal{E}_S , via feature-level distillation on an unlabeled 3D volume \mathbf{x}_u . First, we pass the data through the student encoder to extract its deepest feature map, $\mathbf{F}_S = \mathcal{E}_S(\mathbf{x}_u) \in \mathbb{R}^{C_S \times D_S \times H_S \times W_S}$. To obtain a corresponding representation from the 2D teacher, we process the volume slice-by-slice, stacking the resulting deep feature maps from \mathcal{E}_T into a 3D teacher volume, \mathbf{F}_T . To harmonize these representations, we spatially align \mathbf{F}_T via adaptive average pooling and use a lightweight 3D convolutional projector, \mathcal{P} , to map the student’s feature channels C_S to the teacher’s dimension C_T . The distillation is driven by minimizing the mean squared error between their L2-normalized features, defining our distillation loss $\mathcal{L}_{distill}$ as:

$$\mathcal{L}_{distill} = \left| \frac{\mathcal{P}(\mathcal{E}_S(\mathbf{x}_u))}{\|\mathcal{P}(\mathcal{E}_S(\mathbf{x}_u))\|_2} - \frac{\text{sg}(\mathbf{F}_T)}{\|\text{sg}(\mathbf{F}_T)\|_2} \right|_2^2 \quad (1)$$

where $\text{sg}(\cdot)$ denotes the stop-gradient operator, ensuring the teacher’s weights remain frozen.

The mechanism of this distillation loss directly subverts the confirmation bias cycle. Consider a rare but visually distinct structure where the student’s predictive confidence is low. While a conventional SSL method would generate a weak or incorrect pseudo-label, our DINOv3 teacher, recognizing the region’s unique texture and shape, provides a strong and consistent feature representation. Minimizing $\mathcal{L}_{distill}$ therefore creates a powerful and persistent gradient that forces the student to learn meaningful features for this minority class. This external semantic guidance ensures that all visually distinct regions receive robust supervision, fundamentally preventing the catastrophic representational collapse that plagues inward-looking SSL frameworks.

Progressive Imbalance-aware CutMix (PIC)

A significant challenge in multi-organ medical image segmentation is class imbalance, where standard data augmentations fail to provide sufficient exposure to rare classes. To address this, we propose Progressive Imbalance-aware CutMix (PIC), a dynamic data mixing strategy that adapts its behavior as the model trains. The core principle is to primarily focus on the under-represented classes, forcing the model to refine its decision boundaries for these critical, tail classes. When the model’s capability of recognizing all classes is well established, the exploration is gradually shifted to class-agnostic. Therefore, PIC samples patches uniformly from all classes, allowing the model to learn stable, general features. This progressive shift is governed by a carefully formulated sampling distribution. First, we quantify the class imbalance from the labeled dataset. Let N_c be the total pixel count for class c in a representative subset of the labeled data. We compute an Imbalance Ratio (IR) for each class as:

$$I_c = \frac{\min_j N_j}{N_c}. \quad (2)$$

This assigns a value of 1.0 to the rarest class and smaller values to more frequent ones. From this, we derive a static, class-balanced probability distribution P_{bal} that emphasizes tail classes, controlled by a focusing parameter γ :

$$P_{bal}(c) = \frac{(I_c)^\gamma}{\sum_{j=0}^{C-1} (I_j)^\gamma}, \quad (3)$$

where C is the total number of classes. A higher γ further sharpens the distribution towards minority classes. The PIC module dynamically interpolates between P_{bal} and a uniform distribution P_{uni} as training evolves. The final sampling probability distribution P_E at epoch E is defined as:

$$P_E = (1 - \alpha_t) \cdot P_{bal} + \alpha_t \cdot P_{uni}, \quad \alpha_t = \min \left(1, \frac{E}{\eta * E_{max}} \right). \quad (4)$$

At the start of training ($E \approx 0$), the progressive factor α_t is near zero, making P_E is governed by the class-balancing distribution P_{bal} . As E approaches the scaled maximum number of epochs $\eta * E_{max}$, α_t converges to one, and the sampling follows the uniform distribution P_{uni} . The scaling hyperparameter η controls the shifting speed, where a larger number leads to slower shifting towards the uniform distribution. For each application, a voxel of a target class is sampled from P_E , and a rectangular patch region is formed with the sampled voxel as center. Then, we cut the region from a labeled image and pasted onto a strongly-augmented unlabeled image. This progressive shift creates a stable and effective learning trajectory, improving performance in class-imbalanced, semi-supervised environments.

Optimization

The DINO-Mix framework is trained end-to-end by minimizing a composite loss function that integrates supervised signals, consistency regularization, and external knowledge distillation. The total loss \mathcal{L}_{total} is defined as a weighted sum of three components:

$$\mathcal{L}_{total} = \mathcal{L}_{sup} + \mathcal{L}_{sup}^{aux} + \mathcal{L}_{distill} + \lambda_{unsup} (\mathcal{L}_{unsup} + \mathcal{L}_{unsup}^{aux}), \quad (5)$$

where λ_{sup} is the hyperparameter that balances the unsupervised loss terms. The supervised loss, \mathcal{L}_{sup} and \mathcal{L}_{unsup} are calculated on labeled data \mathbf{x}_l and the PIC mixed image \mathbf{x}_{mix} , with the segmentation loss (combined Dice and Cross-Entropy). \mathcal{L}_{sup}^{aux} and $\mathcal{L}_{unsup}^{aux}$ are the masked segmentation loss that aims to balance the classes following (Zhang et al. 2025). Finally, the distillation loss $\mathcal{L}_{distill}$ is defined in Equation 1, which aligns the student’s feature representation of \mathbf{x}_{mix} with the frozen DINOv3 teacher’s representation, thereby injecting unbiased semantic guidance into the training process of the model.

Experiments

Datasets

Synapse dataset. The Synapse dataset provides 30 axial contrast-enhanced abdominal CT scans for multi-organ segmentation. It features 13 distinct foreground classes: spleen (Sp), right kidney (RK), left kidney (LK), gallbladder (Ga),

Table 1: Results on Synapse dataset with 20% labeled data. ‘General’ or ‘Imbalance’ indicates whether the methods consider the imbalance issue or not. Sp: spleen, RK: right kidney, LK: left kidney, Ga: gallbladder, Es: esophagus, Li: liver, St: stomach, Ao: aorta, IVC: inferior vena cava, PSV: portal & splenic veins, Pa: pancreas, RAG: right adrenal gland, LAG: left adrenal gland. Results of 3-times repeated experiments are reported in the ‘mean±std’ format. Best results are boldfaced.

Methods	Avg. Dice	Avg. ASD	Dice of Each Class												
			Sp	RK	LK	Ga	Es	Li	St	Ao	IVC	PSV	Pa	RAG	LAG
V-Net (fully)	62.09±1.2	10.28±3.9	84.6	77.2	73.8	73.3	38.2	94.6	68.4	72.1	71.2	58.2	48.5	17.9	29.0
General	UA-MT (MICCAI’19)	20.26±2.2	71.67±7.4	48.2	31.7	22.2	0.0	0.0	81.2	29.1	23.3	27.5	0.0	0.0	0.0
	URPC (MICCAI’21)	25.68±5.1	72.74±15.5	66.7	38.2	56.8	0.0	0.0	85.3	33.9	33.1	14.8	0.0	5.1	0.0
	CPS (CVPR’21)	33.55±3.7	41.21±9.1	62.8	55.2	45.4	35.9	0.0	91.1	31.3	41.9	49.2	8.8	14.5	0.0
	SS-Net (MICCAI’22)	35.08±2.8	50.81±6.5	62.7	67.9	60.9	34.3	0.0	89.9	20.9	61.7	44.8	0.0	8.7	4.2
	DST (NeurIPS’22)	34.47±1.6	37.69±2.9	57.7	57.2	46.4	43.7	0.0	89.0	33.9	43.3	46.9	9.0	21.0	0.0
	DePL (CVPR’22)	36.27±0.9	36.02±0.8	62.8	61.0	48.2	54.8	0.0	90.2	36.0	42.5	48.2	10.7	17.0	0.0
Imbalance	Adsh (ICML’22)	35.29±0.5	39.61±4.6	55.1	59.6	45.8	52.2	0.0	89.4	32.8	47.6	53.0	8.9	14.4	0.0
	CRest (CVPR’21)	38.33±3.4	22.85±9.0	62.1	64.7	53.8	43.8	8.1	85.9	27.2	54.4	47.7	14.4	13.0	18.7
	SimiS (arXiv’22)	40.07±0.6	32.98±0.5	62.3	69.4	50.7	61.4	0.0	87.0	33.0	59.0	57.2	29.2	11.8	0.0
	Basak (MICCAI’22)	33.24±0.6	43.78±2.5	57.4	53.8	48.5	46.9	0.0	87.8	28.7	42.3	45.4	6.3	15.0	0.0
	CLD (MICCAI’22)	41.07±1.2	32.15±3.3	62.0	66.0	59.3	61.5	0.0	89.0	31.7	62.8	49.4	28.6	18.5	0.0
	DHC (MICCAI’23)	48.61±0.9	10.71±2.6	62.8	69.5	59.2	66.0	13.2	85.2	36.9	67.9	61.5	37.0	30.9	31.4
	A&D (NeurIPS’23)	60.88±0.7	2.52±0.4	85.2	66.9	67.0	52.7	62.9	89.6	52.1	83.0	74.9	41.8	43.4	44.8
	SKCDF (CVPR’25)	64.27±1.4	1.45±0.1	79.5	72.1	67.6	59.8	60.7	93.3	61.7	85.4	78.5	41.8	50.9	46.4
	DINO-Mix (Ours)	66.45±0.1	1.27±0.1	89.0	73.3	71.8	68.7	64.0	94.4	59.4	86.2	79.0	48.6	45.6	47.3

esophagus (Es), liver (Li), stomach (St), aorta (Ao), inferior vena cava (IVC), portal & splenic veins (PSV), pancreas (Pa), right adrenal gland (RAG), and left adrenal gland (LAG), alongside a ubiquitous background class. For consistency with prior work (Wang and Li 2023a; Zhang et al. 2025), all scans were resampled to a uniform dimension of $80 \times 160 \times 160$ voxels. The dataset was subsequently divided randomly into a training set of 20 scans, a validation set of 4 scans, and a test set of 6 scans. To ensure robustness against data sampling variability inherent to the limited dataset size, experiments on Synapse were conducted three times with independent random seeds.

AMOS dataset. The AMOS dataset presents a broader scope with 360 scans and a modified set of anatomical structures compared to Synapse. Specifically, it excludes the portal & splenic veins (PSV) but incorporates duodenum (Du), bladder (Bl), and prostate/uterus (P/U) as new classes. The dataset’s partitioning yields 216 scans for training, 24 for validation, and 120 for testing.

Implementation Details

We conduct our experiments using PyTorch 2.4.0, CUDA 12.4. The network is a simple VNet architecture (Milletari, Navab, and Ahmadi 2016), with parameters optimized with SGD with a momentum of 0.9 and an initial learning rate (lr) of 0.1 with momentum 0.9 and weight decay 3e-5. In the training stage, we randomly crop a volume of size $64 \times 128 \times 128$. Random gamma augmentation is applied as the additional strong augmentation, and the ema weight is set to 0.99. The λ_{unsup} is set to 0.5 during training. We train the networks for $E_{max} = 1500$ epochs with a batch size of 4, consisting of 2 labeled and 2 unlabeled data. In the inference stage, only the VNet (Milletari, Navab, and Ahmadi 2016) is utilized for prediction, thus *no additional computa-*

tation is required. Final segmentation results are obtained using a sliding window strategy with a stride size of $32 \times 32 \times 16$. For evaluation, we utilize two common metrics: the Dice Score (%) and the Average Surface Distance (ASD) in voxels. The Dice Score quantifies the percentage of overlap between the predicted segmentation and the ground truth, while the ASD measures the average distance between their respective boundaries.

Comparison with State-of-the-art Methods

We rigorously compared our method against a suite of state-of-the-art semi-supervised segmentation techniques (Yu et al. 2019; Luo et al. 2021b; Chen et al. 2021; Wu et al. 2022; Chen et al. 2022a; Wang et al. 2022), including those specifically developed to address class-imbalance challenges (Guo and Li 2022; Wei et al. 2021; Chen et al. 2022b; Basak, Ghosal, and Sarkar 2022; Lin et al. 2022; Wang and Li 2023a,b; Zhang et al. 2025).

Our initial evaluation was performed on the Synapse dataset with a challenging scenario of only 20% labeled data. As detailed in Table 1, general semi-supervised methods have poor segmentation performance on small organs. Existing class-imbalance semi-supervised medical image segmentation methods yielded some improvements for minority classes but still struggle with the inherent class imbalance. Compared with them, our proposed approach demonstrates clear superiority. Specifically, DINO-Mix achieves a new state-of-the-art average Dice score of 66.45% and an average ASD of 1.27, significantly outperforming the next-best method, SKCDF (64.27% Dice, 1.45 ASD). This represents an absolute improvement of 2.18% in Dice and a relative reduction of 12.4% in ASD, demonstrating the enhanced accuracy and boundary precision of our model. Notably, DINO-Mix shows marked improvements in segmenting complex

Table 2: Results on AMOS dataset with 5% labeled data. Sp: spleen, RK: right kidney, LK: left kidney, Ga: gallbladder, Es: esophagus, Li: liver, St: stomach, Ao: aorta, IVC: inferior vena cava, Pa: pancreas, RAG: right adrenal gland, LAG: left adrenal gland, Du: duodenum, Bl: bladder, P/U: prostate/uterus. Best results are boldfaced.

Method	Avg. Dice	Avg. ASD	Dice of Each Class																
			Sp	RK	LK	Ga	Es	Li	St	Ao	IVC	Pa	RAG	LAG	Du	Bl	P/U		
VNet (fully) 2016	76.50	2.01	92.2	92.2	93.3	65.5	70.3	95.3	82.4	91.4	85.0	74.9	58.6	58.1	65.6	64.4	58.3		
General	UA-MT (MICCAI'19)	42.16	15.48	59.8	64.9	64.0	35.3	34.1	77.7	37.8	61.0	46.0	33.3	26.9	12.3	18.1	29.7	31.6	
	URPC (MICCAI'21)	44.93	27.44	67.0	64.2	67.2	36.1	0.0	83.1	45.5	67.4	54.4	46.7	0.0	29.4	35.2	44.5	33.2	
	CPS (CVPR'21)	41.08	20.37	56.1	60.3	59.4	33.3	25.4	73.8	32.4	65.7	52.1	31.1	25.5	6.2	18.4	40.7	35.8	
	SS-Net (MICCAI'22)	33.88	54.72	65.4	68.3	69.9	37.8	0.0	75.1	33.2	68.0	56.6	33.5	0.0	0.0	0.0	0.2	0.2	
	DST (NeurIPS'22)	41.44	21.12	58.9	63.3	63.8	37.7	29.6	74.6	36.1	66.1	49.9	32.8	13.5	5.5	17.6	39.1	33.1	
	DePL (CVPR'22)	41.97	20.42	55.7	62.4	57.7	36.6	31.3	68.4	33.9	65.6	51.9	30.2	23.3	10.2	20.9	43.9	37.7	
Imbalance	Adsh (ICML'22)	40.33	24.53	56.0	63.6	57.3	34.7	25.7	73.9	30.7	65.7	51.9	27.1	20.2	0.0	18.6	43.5	35.9	
	CReST (CVPR'21)	46.55	14.62	66.5	64.2	65.4	36.0	32.2	77.8	43.6	68.5	52.9	40.3	24.7	19.5	26.5	43.9	36.4	
	SimiS (arXiv'22)	47.27	11.51	77.4	72.5	68.7	32.1	14.7	86.6	46.3	74.6	54.2	41.6	24.4	17.9	21.9	47.9	28.2	
	Basak (MICCAI'22)	38.73	31.76	68.8	59.0	54.2	29.0	0.0	83.7	39.3	61.7	52.1	34.6	0.0	0.0	26.8	45.7	26.2	
	CLD (MICCAI'22)	46.10	15.86	67.2	68.5	71.4	41.0	21.0	76.1	42.4	69.8	52.1	37.9	24.7	23.4	22.7	38.1	35.2	
	DHC (MICCAI'23)	49.53	13.89	68.1	69.6	71.1	42.3	37.0	76.8	43.8	70.8	57.4	43.2	27.0	28.7	29.1	41.4	36.7	
	A&D (NeurIPS'23)	50.03	5.21	73.1	76.0	76.5	29.1	44.9	82.5	49.0	72.8	61.7	48.5	30.2	19.7	36.4	32.9	18.2	
	SKCDF (CVPR'25)	53.81	5.97	77.1	77.9	71.2	34.1	50.4	88.6	51.6	80.9	58.9	48.8	33.0	30.2	32.2	45.9	26.4	
DINO-Mix (Ours)			62.73	3.28	85.9	85.6	85.4	39.2	59.6	90.1	62.5	86.9	74.2	60.2	44.0	38.9	44.1	50.3	34.1

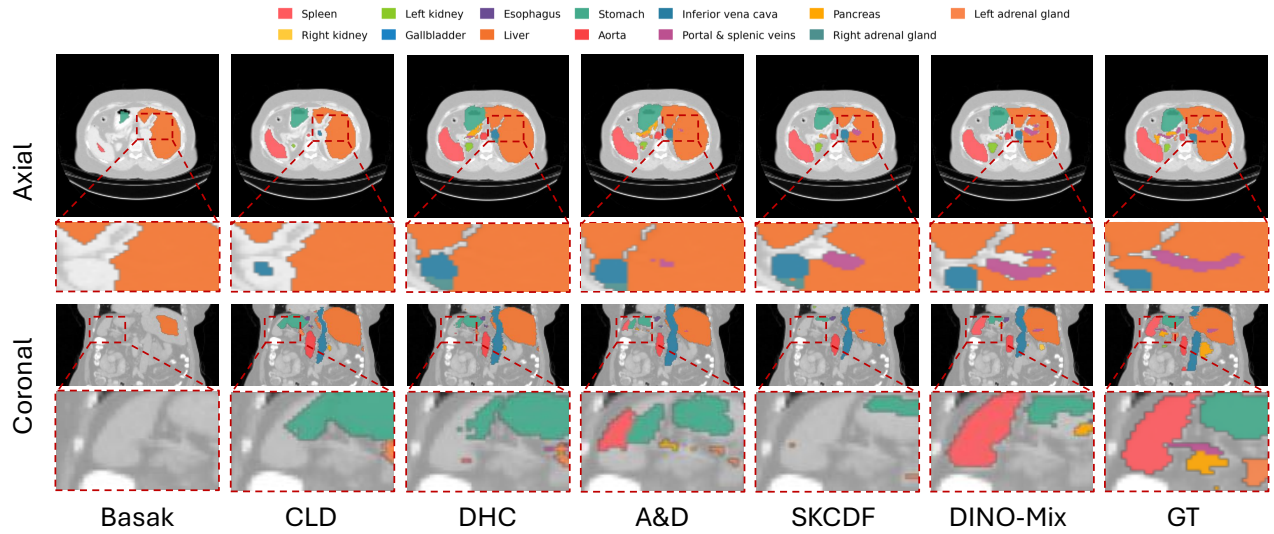


Figure 2: Qualitative comparison between our proposed DINO-Mix and the state-of-the-art semi-supervised class-imbalanced medical image segmentation methods on 20% labeled Synapse dataset.

structures, boosting the Dice score for the Portal & Splenic Veins (PSV) by 6.8% (from 41.8% to 48.6%) and the Spleen (Sp) by 9.5% (from 79.5% to 89.0%) compared to the previous state-of-the-art. Furthermore, it is observed that our method shows surprisingly robust performance across multiple runs, with merely 0.1 standard deviation on both Dice and ASD, which could suggest that our proposed FKD enables the model to learn robust representations.

To further affirm the robustness and generalizability of our framework, we extended our evaluation to the more complex AMOS dataset, using an even more restricted 5% labeled data setting. The results, presented in Table 2, reinforce the consistent advantages of our method. DINO-Mix once again sets a new performance benchmark with a lead-

ing average Dice score of 62.73% and an ASD of 3.28. This constitutes a substantial improvement of 8.92% in absolute Dice score over the strongest prior method (53.81%). The performance gains are particularly pronounced for challenging organs that suffer from class imbalance, such as the Pancreas (Pa), which saw its Dice score increase by 11.4% (from 48.8% to 60.2%), and the Stomach (St), with a 10.9% increase (from 51.6% to 62.5%). These consistent and significant gains across two distinct datasets and under different limited-label scenarios highlight the effectiveness and reliability of our proposed DINO-Mix framework. We present a qualitative comparison of various methods in Fig. 2. Existing methods frequently exhibit tendencies toward producing false segmentation regions or ignoring smaller anatomical

Table 3: Ablation of the proposed components on the Synapse dataset with 20% labeled data. Consist means the proposed consistency regularization based baseline framework. Results of 3-times repeated experiments are reported.

Consist	FKD	PIC	Aux	Avg.	Avg.	Dice of Each Class												
				Dice	ASD	Sp	RK	LK	Ga	Es	Li	St	Ao	IVC	PSV	PA	RAG	LAG
✓				48.14±1.2	7.07±3.2	76.1	64.8	60.3	50.2	0.0	93.3	45.0	82.9	76.5	30.0	39.7	0.0	7.1
✓	✓			54.72±0.1	6.12±0.2	79.2	71.4	54.5	51.1	53.3	92.5	45.6	82.7	75.8	36.1	39.1	0.0	30.2
✓		✓		64.97±3.4	1.39±0.2	87.2	66.7	70.5	63.6	63.3	94.1	60.1	84.9	77.1	50.0	45.3	46.1	35.6
✓	✓	✓		66.31±0.2	1.28±0.2	90.2	73.4	73.5	67.0	64.4	94.5	62.1	86.4	79.8	48.2	45.9	44.6	31.9
✓	✓	✓	✓	66.45±0.1	1.27±0.1	89.0	73.3	71.8	68.7	64.0	94.4	59.4	86.2	79.0	48.6	45.6	47.3	36.6

Table 4: Performance comparison with varied scaling parameter η in PIC on 20% labeled Synapse dataset.

η	Avg. Dice	Avg. ASD
0	64.87 ± 0.9	3.02 ± 0.5
1/2	65.96 ± 1.1	1.34 ± 0.2
2/3	66.45 ± 0.1	1.27 ± 0.1
∞	65.75 ± 0.2	1.57 ± 0.2

structures. Our proposed approach consistently yields more precise and anatomically faithful delineations for these challenging minority organs.

Ablation Studies

Ablation on the components To validate the contribution of each component, we performed an ablation study on the Synapse dataset in Table 3. The consistency regularization baseline achieves a 48.14% mean Dice and suffers from the segmentation on several minority classes, which suggests the issue of confirmation bias. Integrating FKD significantly improves performance to 54.72% Dice by introducing an unbiased external teacher, which proves crucial for external knowledge in learning underrepresented classes. Separately, adding PIC yields a leap to 64.97% Dice by enforcing a dynamic curriculum focused on minority classes. The combination of FKD and PIC further boost performance to 66.31%, demonstrating their synergistic effect, where the PIC-enhanced student better absorbs the knowledge from the FKD teacher. Finally, including an auxiliary head (Lee, Shin, and Kim 2021; Zhang et al. 2025) brings a peak performance of 66.45% mean Dice, confirming that each component is a valuable contributor to DINO-Mix framework.

Ablation on the scaling parameter η The scaling parameter η dictates the speed of the transition from a class-balanced (P_{bal}) to a uniform (P_{uni}) sampling distribution. In Table 4, our ablation study on the Synapse dataset reveals the importance of a well-paced transition. The extreme cases, employing a purely uniform ($\eta = 0$) or a purely class-balanced ($\eta = \infty$) strategy throughout training, both yield suboptimal results. The purely uniform approach performed the worst, suggesting the necessity of an initial phase of balanced sampling. Conversely, relying solely on class-balancing hindered the model’s ability to adapt to the natural data distribution. The optimal performance in terms of both Dice and ASD was achieved with $\eta = 2/3$. This result

Table 5: Performance comparison with different choices of foundational model on 20% labeled Synapse dataset.

Model	Avg. Dice	Avg. ASD
DINOv2 (Oquab et al. 2023)	65.86 ± 0.3	1.41 ± 0.2
DINOv3 (Siméoni et al. 2025)	66.45 ± 0.1	1.27 ± 0.1
CLIP (Radford et al. 2021)	64.26 ± 1.0	1.49 ± 0.7
SigLIP2 (Tschannen et al. 2025)	65.72 ± 0.1	1.32 ± 0.4

validates our PIC strategy, which allows the model to first learn robust features for all classes, including rare ones, before gradually shifting to an uniform distribution. This moderately paced transition strikes the most effective balance.

Ablation on the choice of foundational model We ablated four prominent foundational models and summarize the results in Table 5. DINOv3 yields the best performance, achieving a superior Dice score of 66.45% and the lowest Average ASD of 1.27. While DINOv2 and SigLIP2 also proved to be effective, they did not reach the performance level of DINOv3. The vision-language model CLIP resulted in the lowest performance (64.26% Dice) and showed considerable instability. We hypothesize that the purely visual, self-supervised pre-training objective of the DINO models enables them to learn more generalizable and robust feature representations of fundamental concepts like shape and texture, which are critical for providing an unbiased supervisory signal in medical imaging. In contrast, the vision language models may be more aligned with textual semantics, making them less suitable for this dense prediction task. Therefore, we selected DINOv3 as the frozen teacher encoder for all experiments.

Conclusion

In this work, we addressed the critical failure of conventional “inward-looking” semi-supervised frameworks, which amplify confirmation bias on imbalanced medical datasets. We proposed DINO-Mix, a novel “outward-looking” paradigm that dismantles this vicious cycle on two synergistic levels. Through Foundational Knowledge Distillation (FKD), we leveraged an external, unbiased DINOv3 teacher to provide a stable semantic anchor for minority classes, defining what to learn. Simultaneously, our Progressive Imbalance-aware CutMix (PIC) curriculum cultivated a more robust student model, mastering how to learn by first confronting

and then generalizing from class imbalances. Our state-of-the-art results on the Synapse and AMOS benchmarks validate this two-pronged strategy, demonstrating the effectiveness of looking outward to harness objective, foundational knowledge for reliable semi-supervised learning.

References

Arazo, E.; Ortego, D.; Albert, P.; O'Connor, N. E.; and McGuinness, K. 2020. Pseudo-labeling and confirmation bias in deep semi-supervised learning. 1–8.

Bai, Y.; Chen, D.; Li, Q.; Shen, W.; and Wang, Y. 2023. Bidirectional Copy-Paste for Semi-Supervised Medical Image Segmentation. In *CVPR*, 11514–11524.

Basak, H.; Ghosal, S.; and Sarkar, R. 2022. Addressing Class Imbalance in Semi-supervised Image Segmentation: A Study on Cardiac MRI. In *MICCAI*, 224–233.

Chen, B.; Jiang, J.; Wang, X.; Wan, P.; Wang, J.; and Long, M. 2022a. Debiased Self-Training for Semi-Supervised Learning.

Chen, H.; Fan, Y.; Wang, Y.; Wang, J.; Schiele, B.; Xie, X.; Savvides, M.; and Raj, B. 2022b. An Embarrassingly Simple Baseline for Imbalanced Semi-Supervised Learning. *arXiv preprint arXiv:2211.11086*.

Chen, X.; Yuan, Y.; Zeng, G.; and Wang, J. 2021. Semi-supervised semantic segmentation with cross pseudo supervision. In *CVPR*, 2613–2622.

Guo, L.-Z.; and Li, Y.-F. 2022. Class-imbalanced semi-supervised learning with adaptive thresholding. 8082–8094.

Han, K.; Sheng, V. S.; Song, Y.; Liu, Y.; Qiu, C.; Ma, S.; and Liu, Z. 2024. Deep semi-supervised learning for medical image segmentation: A review. *Expert Systems with Applications*, 245: 123052.

Hoyer, L.; Tan, D. J.; Naeem, M. F.; Van Gool, L.; and Tombari, F. 2024. SemiVL: semi-supervised semantic segmentation with vision-language guidance. In *European Conference on Computer Vision*, 257–275. Springer.

Hu, M.; Yin, J.; Ma, Z.; Ma, J.; Zhu, F.; Wu, B.; Wen, Y.; Wu, M.; Hu, C.; Hu, B.; et al. 2025. beta-FFT: Nonlinear Interpolation and Differentiated Training Strategies for Semi-Supervised Medical Image Segmentation. 30839–30849.

Huang, K.; Zhou, Y.; Fu, H.; Zhang, Y.; Gong, C.; and Zhou, T. 2025. Text-driven Multiplanar Visual Interaction for Semi-supervised Medical Image Segmentation. In *International Conference on Medical Image Computing and Computer-Assisted Intervention*, 604–613. Springer.

Lee, H.; Shin, S.; and Kim, H. 2021. Abc: Auxiliary balanced classifier for class-imbalanced semi-supervised learning. *Advances in Neural Information Processing Systems*, 34: 7082–7094.

Li, C.; Liu, X.; Li, W.; Wang, C.; Liu, H.; Liu, Y.; Chen, Z.; and Yuan, Y. 2025. U-kan makes strong backbone for medical image segmentation and generation. In *Proceedings of the AAAI Conference on Artificial Intelligence*, volume 39, 4652–4660.

Li, K.; Liu, X.; and Chen, Z. 2024. Semantic consistency regularization with large language models for semi-supervised sentiment analysis. In *International Conference on Neural Information Processing*, 289–303. Springer.

Li, L.; Lian, S.; Luo, Z.; Wang, B.; and Li, S. 2024. VCLIPSeg: Voxel-Wise CLIP-Enhanced Model for Semi-supervised Medical Image Segmentation. In *International Conference on Medical Image Computing and Computer-Assisted Intervention*, 692–701. Springer.

Li, X.; Huang, Y.; and Guan, Q. 2025. CLIP-driven Coarse-to-fine Semantic Guidance for Fine-grained Open-set Semi-supervised Learning. In *Proceedings of the Computer Vision and Pattern Recognition Conference*, 30312–30321.

Lin, Y.; Yao, H.; Li, Z.; Zheng, G.; and Li, X. 2022. Calibrating label distribution for class-imbalanced barely-supervised knee segmentation. In *MICCAI*, 109–118.

Liu, X.; Chen, Z.; and Yuan, Y. 2024. MOST: multi-formation soft masking for semi-supervised medical image segmentation. In *International Conference on Medical Image Computing and Computer-Assisted Intervention*, 469–480. Springer.

Liu, X.; Li, W.; and Yuan, Y. 2024. Diffrect: Latent diffusion label rectification for semi-supervised medical image segmentation. In *International Conference on Medical Image Computing and Computer-Assisted Intervention*, 56–66. Springer.

Luo, X.; Chen, J.; Song, T.; and Wang, G. 2021a. Semi-supervised medical image segmentation through dual-task consistency. In *Proceedings of the AAAI Conference on Artificial Intelligence*, volume 35, 8801–8809.

Luo, X.; Liao, W.; Chen, J.; Song, T.; Chen, Y.; Zhang, S.; Chen, N.; Wang, G.; and Zhang, S. 2021b. Efficient semi-supervised gross target volume of nasopharyngeal carcinoma segmentation via uncertainty rectified pyramid consistency. In *MICCAI*, 318–329.

Milletari, F.; Navab, N.; and Ahmadi, S.-A. 2016. V-net: Fully convolutional neural networks for volumetric medical image segmentation. In *2016 fourth international conference on 3D vision (3DV)*, 565–571. Ieee.

Oquab, M.; Darcet, T.; Moutakanni, T.; Vo, H.; Szafraniec, M.; Khalidov, V.; Fernandez, P.; Haziza, D.; Massa, F.; El-Nouby, A.; et al. 2023. Dinov2: Learning robust visual features without supervision. *arXiv preprint arXiv:2304.07193*.

Pham, D.-H.; Nguyen, D.-D.; Pham, A.; Ho, T.; Nguyen, P.; Nguyen, K.; and Nguyen, R. 2025. Semi-supervised 3D Semantic Scene Completion with 2D Vision Foundation Model Guidance. In *Proceedings of the AAAI Conference on Artificial Intelligence*, volume 39, 6514–6522.

Radford, A.; Kim, J. W.; Hallacy, C.; Ramesh, A.; Goh, G.; Agarwal, S.; Sastry, G.; Askell, A.; Mishkin, P.; Clark, J.; et al. 2021. Learning transferable visual models from natural language supervision. 8748–8763.

Siméoni, O.; Vo, H. V.; Seitzer, M.; Baldassarre, F.; Oquab, M.; Jose, C.; Khalidov, V.; Szafraniec, M.; Yi, S.; Ramamonjisoa, M.; et al. 2025. Dinov3.

Sohn, K.; Berthelot, D.; Carlini, N.; Zhang, Z.; Zhang, H.; Raffel, C. A.; Cubuk, E. D.; Kurakin, A.; and Li, C.-L. 2020. Fixmatch: Simplifying semi-supervised learning with consistency and confidence. *Advances in neural information processing systems*, 33: 596–608.

Tarvainen, A.; and Valpola, H. 2017. Mean teachers are better role models: Weight-averaged consistency targets improve semi-supervised deep learning results. *Advances in neural information processing systems*, 30.

Tschannen, M.; Gritsenko, A.; Wang, X.; Naeem, M. F.; Alabdulmohsin, I.; Parthasarathy, N.; Evans, T.; Beyer, L.; Xia, Y.; Mustafa, B.; et al. 2025. Siglip 2: Multilingual vision-language encoders with improved semantic understanding, localization, and dense features. *arXiv preprint arXiv:2502.14786*.

Wang, H.; and Li, X. 2023a. DHC: Dual-debiased Heterogeneous Co-training Framework for Class-imbalanced Semi-supervised Medical Image Segmentation. In *MICCAI*, 582–591. Springer.

Wang, H.; and Li, X. 2023b. Towards generic semi-supervised framework for volumetric medical image segmentation. *Advances in Neural Information Processing Systems*, 36: 1833–1848.

Wang, X.; Wu, Z.; Lian, L.; and Yu, S. X. 2022. Debiased Learning from Naturally Imbalanced Pseudo-Labels. 14647–14657.

Wei, C.; Sohn, K.; Mellina, C.; Yuille, A.; and Yang, F. 2021. Crest: A class-rebalancing self-training framework for imbalanced semi-supervised learning. In *CVPR*, 10857–10866.

Wu, Y.; Wu, Z.; Wu, Q.; Ge, Z.; and Cai, J. 2022. Exploring smoothness and class-separation for semi-supervised medical image segmentation. In *MICCAI*, 34–43.

Yang, Q.; Liu, X.; Chen, Z.; Ibragimov, B.; and Yuan, Y. 2022. Semi-supervised medical image classification with temporal knowledge-aware regularization. In *International conference on medical image computing and computer-assisted intervention*, 119–129. Springer.

Yu, L.; Wang, S.; Li, X.; Fu, C.-W.; and Heng, P.-A. 2019. Uncertainty-aware self-ensembling model for semi-supervised 3D left atrium segmentation. In *MICCAI*, 605–613.

Zhang, Z.; Yin, G.; Zhang, B.; Liu, W.; Zhou, X.; and Wang, W. 2025. A Semantic Knowledge Complementarity based Decoupling Framework for Semi-supervised Class-imbalanced Medical Image Segmentation. In *Proceedings of the Computer Vision and Pattern Recognition Conference*, 25940–25949.